Environmental Science Advances

ROYAL SOCIETY OF CHEMISTRY

PAPER

View Article Online
View Journal | View Issue

Cite this: *Environ. Sci.: Adv.*, 2026, **5**, 802

Synthesis of near-infrared-fluorophore-loaded microplastics with different compositions for *in vivo* tracking

Sota Inoue,[a] Ryo Nagasawa,[a] Kohei Soga[ab] and Masakazu Umezawa *[abc]

Microplastics (MPs) are pervasive environmental pollutants of growing concern owing to their potential impact on ecosystems and human health. Although reports of human exposure to MPs are increasing, our understanding of the *in vivo* behavior of MPs remains limited. This study aimed to enable the observation of the *in vivo* dynamics of MPs by loading them with a fluorescent dye that emits light in the second near-infrared (NIR-II) biological window, which allows deep-tissue imaging. Plastic granules—composed of polypropylene, polyethylene, or polystyrene—were dispersed in tetrahydrofuran to generate nanosized particles, which were mixed with a solution of IR-1061 dye in acetonitrile and heated at 55 °C (N_2 atmosphere) to promote dye loading. An aqueous solution of bovine serum albumin was then added dropwise and stirred in open air to evaporate the organic solvent, resulting in obtaining water-dispersed IR-1061-loaded MPs that exhibited fluorescence in the NIR-II region. The *in vivo* behavior of IR-1061-loaded MPs was examined following oral administration to mice. No fluorescence from IR-1061-loaded MPs was observed in tissues outside the gastrointestinal tract, indicating minimal intestinal absorption. At 48 h post-administration, NIR-II fluorescence from IR-1061-loaded MPs was observed in feces but not *in vivo*, indicating that the MPs were excreted in feces. The extent of intestinal retention was influenced by MP size rather than chemical composition. The development of methods for synthesizing NIR-II-fluorophore-loaded MP models with various chemical compositions will support risk assessments by providing insights into the environmental and biological fates of MPs.

Received 14th October 2025
Accepted 28th January 2026

DOI: 10.1039/d5va00360a

rsc.li/esadvances

Environmental significance

Microplastics (MPs) have been a globally distributed environmental problem; however, their *in vivo* behaviors are still largely unclarified. In this study, we present a strategy to visualize and track MPs *in vivo* by labeling them with IR-1061, a fluorophore that emits light in the second near-infrared (NIR-II) biological window, enabling optical imaging in deep tissues. NIR-II-fluorophore-labeled MPs of different chemical compositions enable real-time *in vivo* tracking and provide new insights into their biodistribution, intestinal retention, and excretion pathways—critical parameters for assessing their potential health and environmental impacts. The use of NIR-II fluorescence imaging will contribute to elucidating the *in vivo* behavior of MPs, offering a non-invasive and sensitive method for assessing their biodistribution, and to better understand their risk on human health.

1. Introduction

Microplastics (MPs) are widely recognized as environmental pollutants, with human exposure occurring through various sources, including food, beverages, and airborne particles.[1] The awareness of MPs began in the 1970s, when researchers first identified their presence in marine environments.[2] Global plastic waste is estimated to increase significantly from 188 million tons in 2016 to 380 million tons by 2040.[3] MPs are defined as plastic fragments with a diameter < 5 mm and are commonly found in products such as detergents and cosmetics.[4] Some MPs are manufactured intentionally, whereas others are formed in the environment through the degradation of larger plastic debris caused by mechanical forces (*e.g.*, abrasion and fragmentation) and prolonged exposure to environmental factors such as ultraviolet (UV) radiation and temperature fluctuations.[5–7] MPs found in the environment are predominantly fragments or fibers and consist of various polymers such as poly(ethylene terephthalate) (PET), polypropylene (PP), polyethylene (PE), and polystyrene (PS).[8] PE, PP, and PS

[a]*Department of Materials Science and Technology, Graduate School of Advanced Engineering, Tokyo University of Science, Niijuku 6-3-1, Katsushika, Tokyo 125-8585, Japan. E-mail: masa-ume@rs.tus.ac.jp*

[b]*Department of Medical and Robotic Engineering Design, Faculty of Advanced Engineering, Tokyo University of Science, Niijuku 6-3-1, Katsushika, Tokyo 125-8585, Japan*

[c]*Division of Smart Healthcare Engineering, Research Institute for Science and Technology (RIST), Tokyo University of Science, 2641 Yamazaki, Noda, Chiba 278-8510, Japan*

have densities lower than those of seawater, making them more likely to float and persist on the ocean surface.[9]

Exposure to MPs can occur *via* ingestion or inhalation. Dietary intake is estimated to be 107–142 particles per day, with a maximum ingestion of 5 g per week.[10] A meta-analysis assessing human exposure reported that adults may ingest an average of 258–312 particles per day.[11] MPs have been detected in various sources, including fruits and vegetables,[12] seafood,[13] drinking water,[14] and table salt.[15] In addition, they have been detected in human blood[16] and feces;[17] however, the mechanism by which they enter the human body and their potential effects remains poorly understood.[18] Understanding the mechanisms of accumulation and dynamics of MPs within biological tissues and organs is essential for assessing their potential health impacts.[19] Conventional detection techniques such as Fourier transform infrared spectroscopy and Raman spectroscopy enables the quantitative analysis of MPs.[20] Fluorescence imaging[21] and hyperspectral stimulated Raman scattering microscopy[22] have been developed for tracking the distribution of MPs. However, these methods are limited to excised organs and cannot track the real-time dynamics of MPs in living tissues; therefore, most detection techniques face limitations when analyzing biological samples.[23]

To address this limitation, this study leveraged the potential of near-infrared fluorescence (NIRF) imaging in the over-thousand-nanometers (OTN) range, known as the second NIR (NIR-II) biological window.[24] Unlike shorter wavelengths, NIR light in the OTN range exhibits reduced scattering *in vivo*, enabling the dynamic imaging of particles located deep within the tissues.[25] Fluorescence imaging in NIR-II wavelength region expands the observation depth from several millimeters in visible and shorter wavelength NIR (NIR-I; <1000 nm) to 1–2 centimeters in biological tissues.[26,27] Compared with magnetic resonance imaging, which requires the incorporation of magnetic elements into MPs,[28] OTN-NIRF imaging offers a simple alternative for tracking dye-loaded MPs using an optical imaging system. This study developed NIR-II fluorophore-loaded MP model to enable the tracking of MPs in living tissues. Our previous studies have outlined methods for synthesizing NIR-II-fluorophore-loaded PET MPs.[29] In this study, we extended these methods to synthesize PP, PS, and PE MPs loaded with IR-1061, a fluorescent dye emitting in the NIR-II region (1100 nm). This chemically diverse set of dye-loaded MP models was designed to mimic the composition of environmentally prevalent MPs. The development of methods for monitoring NIR-II-fluorophore-loaded MPs represents a significant step toward understanding and visualizing the biological fate of MPs *in vivo*.

2. Materials and methods

2.1. Materials

PP, PE, and PS granules, IR-1061, and bovine serum albumin (BSA) were purchased from Sigma-Aldrich (St Louis, MO, USA). Tetrahydrofuran (THF) and acetonitrile (ACN) were purchased from Fujifilm Wako Pure Chemical Industries (Osaka, Japan). Phosphate-buffered saline (PBS) was purchased from Otsuka Pharmaceutical Factory, Inc. (Tokushima, Japan). All reagents were used without purification.

2.2. Preparation of IR-1061-loaded PP, PE, and PS particles that fluoresce in the NIR-II region

The PP, PE, and PS granules were fragmented into nanosized particles (nearly dissolved) by stirring in THF for 14 days. The obtained THF-dispersed PP, PE, and PS (3 mg mL^{-1}, 2 mL) were then mixed with an IR-1061 solution in ACN (0.7 mg mL^{-1}) and stirred under a nitrogen atmosphere at 55 °C for 1 h (Fig. 1). This process enabled the incorporation of 3–24 μg of IR-1061 into 6 mg of the plastic materials (PP, PE, and PS). After stirring, the mixture was immediately cooled in ice water. Subsequently, an aqueous BSA solution (6 mg mL^{-1}, 1 mL) was added dropwise, and the solution was stirred in an open system for 48 h to facilitate the evaporation of organic solvents (Fig. 1). BSA was added to stabilize the MPs in aqueous media. The resulting product was water-dispersible IR-1061-loaded MPs that fluoresced in the NIR-II region.

2.3. Characterization of IR-1061-loaded PP, PE, and PS particles that fluoresce in the NIR-II region

The fluorescence of IR-1061-loaded PP, PE, and PS particles was analyzed using an NIR spectrometer (NIR Quest, Hanamura Optics, Kanagawa, Japan) under irradiating the samples with 980 nm excitation light from a fiber-coupled diode (SP-976-5-1015-7; Laser Components GmbH, Olching, Germany). The particle size distributions of IR-1061-loaded MPs were determined using dynamic light scattering (DLS; ELSZ-2000ZS, Otsuka Electronic Co., Osaka, Japan).

2.4. Evaluation of the *in vitro* stability of IR-1061-loaded MPs that fluoresce in the NIR-II region

To assess the *in vitro* stability of IR-1061-loaded MPs that fluoresce in the NIR-II region, we measured their fluorescence intensities in PBS. The IR-1061-loaded MPs (1.5 mg mL^{-1}) were dispersed in PBS (pH 7.4). The fluorescence intensity was analyzed using an NIR fluorescence imaging system SAI-1000 (Shimadzu Co., Kyoto, Japan) under 980 nm optical excitation (2.4 W).

2.5. *In vivo* NIR-II fluorescence imaging

For *in vivo* imaging, IR-1061-loaded PP, PE, and PS particles (6 mg mL^{-1}, 0.2 mL) were orally administered to eight-week-old female BALB/c nu/nu mice (Japan SLC, Inc., Shizuoka, Japan). NIR-II fluorescence imaging was performed using the SAI-1000 imaging system under 980 nm optical excitation (power density: 250 mW cm^{-2}, integration time: 500 ms). Animal care and experiments were performed in accordance with the Tokyo University of Science Guidelines for the Care and Use of Laboratory Animals with the approval of the Institutional Animal Care Committee. NIR-II fluorescence intensities in the region of

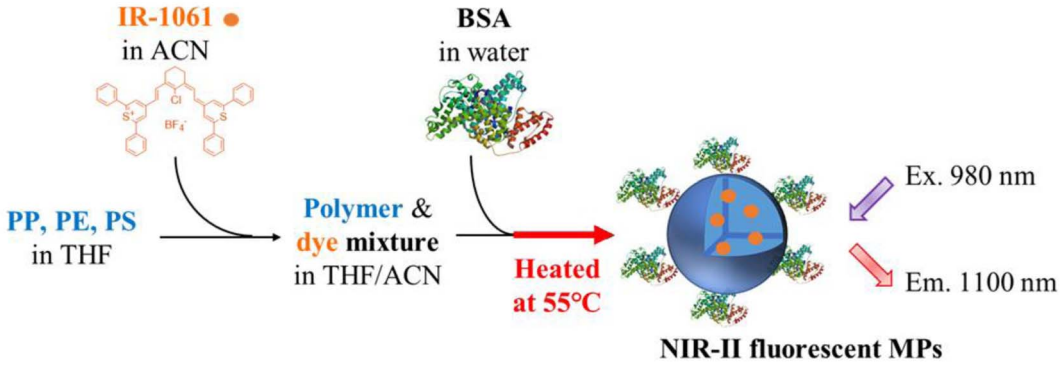

Fig. 1 Schematic of the preparation of IR-1061-loaded PP, PE, or PS fluorescing in the NIR-II region.

interest (stomach and intestines) were semi-quantified by analysis of the grayscale NIR images using ImageJ software.

3. Results and discussion

3.1. Optimization of the IR-1061 loading concentration on the PP, PE, and PS particles

To prepare NIR-II-fluorophore-loaded MP models suitable for *in vivo* tracking, we optimized the loading conditions of the IR-1061 dye to synthesize highly fluorescent IR-1061-loaded PP, PE, and PS particles. To optimize dye loading for the synthesis of MP models labeled with NIR-II fluorophores, we considered the solubility and compatibility of IR-1061 with plastic matrices. Hydrophobic fluorescent dyes such as IR-1061, which have high affinity for polymers, can be introduced into plastics using organic solvents. IR-1061 is soluble in organic solvents such as ACN and THF,[30] making these solvents suitable for dye incorporation in plastics. IR-1061-loaded PET MPs can be synthesized by mixing a solution of IR-1061 in ACN and PET particles, enabling the dye to be incorporated into the plastic particles.[29] However, mixing a solution of IR-1061 in ACN and PP, PP, or PS was insufficient to produce IR-1061-loaded PP, PE, and PS particles. Therefore, a method is required to facilitate dye incorporation into the polymer molecular network, in which compatibility between the dye and the host material is crucial.[31] The solubility parameter (SP) of PET (10.7) is close to that of ACN (SP = 11.9) and compatible with IR-1061.[30] Consequently, dye loading on PET particles can be achieved through simple swelling of PET and diffusion of the dye, which is facilitated by ACN.[29] In contrast, PP and PE, and PS[32] are less polar and therefore exhibit lower SP values than PET. To address this challenge, we exploited the thermal expansion properties of PP, PE, and PS.[33] The mixture of IR-1061 in ACN and the plastic particles was heated at 55 °C to promote the incorporation of IR-1061 into the plastics. The preparation method with albumin protein, a weak surfactant, has an advantage to produce nano- and MPs with irregularly shapes[29,34] that can mimic environmental MPs rather than spherical particles. Albumin protein is essential for the particle preparation; in contrast, large lumps of plastics are only formed *via* precipitation following the preparation process in the absence of BSA. Amide I and II bands attributed to BSA are observed in the MPs prepared by the protocol shown in this study.[34] The resulting MPs were well dispersed by coating with BSA in aqueous media, where the albumin protein also works as microorganism layer mimicking environmental MPs.

As shown in Fig. 2, the fluorescence intensity of IR-1061-loaded PP, PE, and PS particles increased as the dye loading increased from 3 to 24 μg, confirming the effectiveness of the thermal-assisted loading method. The IR-1061 dye was loaded inside the MPs (not on MPs surface), because the resulting plastic particles would not show NIRF if the dye was not introduced into inside but just located near the particle surface.[35]

3.2. Fluorescence retention of IR-1061-loaded PP, PE, and PS particles over time

The fluorescence retention of IR-1061-loaded PP, PE, and PS particles that fluoresce in the NIR-II region was evaluated over time. The IR-1061-loaded PP, PE, and PS MPs retained >80% of their initial fluorescence intensity for 30 d (Fig. 3), indicating high fluorescence retention suitable for *in vivo* tracking and continuous detection in organs over time following absorption.

3.3. *In vivo* NIR-II fluorescence imaging in mice

The *in vivo* behavior of MPs was visualized following the oral administration of IR-1061-loaded MPs (1.2 mg) to mice (Fig. 4). The IR-1061-loaded MPs remained in the stomach for up to 8 h after administration and then migrated to the intestines (Fig. 4 and 5). No fluorescence was detected in tissues outside the gastrointestinal tract, indicating that the intestinal absorption of MPs was negligible. At 48 h post-administration, fluorescence signals were detected in feces rather than *in vivo* tissues, indicating that orally-administered IR-1061-loaded MPs were excreted in feces (Fig. 6). The difference in intestinal retention may be dependent on the chemical composition of MPs, but also be affected by MP size. Among the tested MPs, the PP particles were the smallest (<100 nm, as determined by DLS), whereas the PE and PS particle were larger. The small PP particles exhibited delayed excretion, consistent with previous studies indicating that smaller MPs have a longer gastrointestinal residence time.[1,20] Further investigations are needed to compare the *in vivo* behaviors of MPs with different

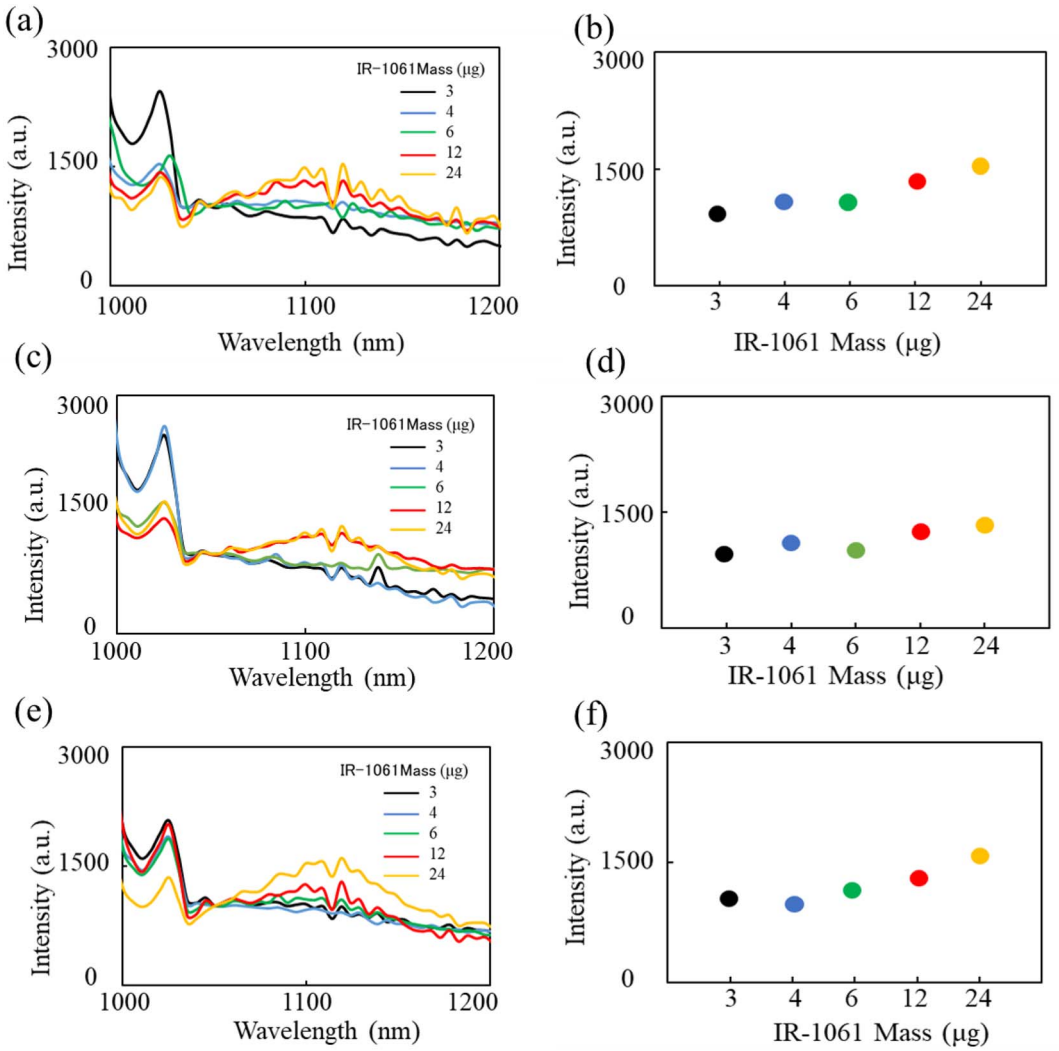

Fig. 2 Fluorescence intensity of IR-1061-loaded PP, PE, and PS MPs at varying dye concentrations. Fluorescence measurement of IR-1061-loaded (a and b) PP, (c and d) PE, and (e and f) PS particles (6 mg mL^{-1}) were obtained under 980 nm excitation light. (a, c and e) Fluorescence spectra and (b, d and f) fluorescence intensity at 1100 nm.

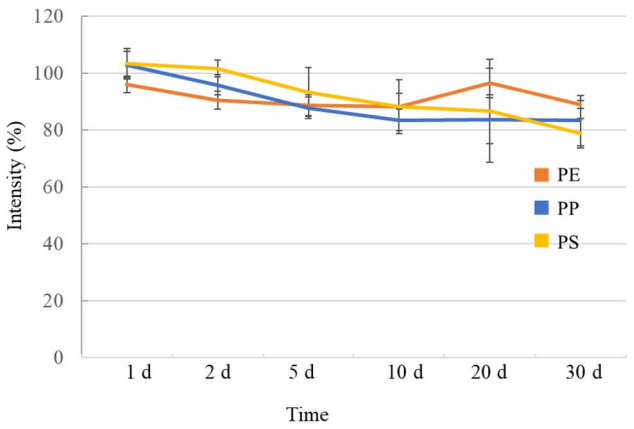

Fig. 3 Fluorescence retention of IR-1061-loaded MPs over time, normalized to initial intensity after MP preparation.

compositions and similar sizes potentially controlled by additive BSA concentration for preparation.[29]

Some limitations merit discussion regarding this study, first, only the hairless mice were used for *in vivo* experiments of the NIR-II fluorescence imaging of MPs in deep tissues without scattering by the hair. The biological effects of MPs should be investigated using other strains with immune responses in normal physiology in further investigations. Second, although the stability of IR-1061 loaded to our MPs was suggested by the observation of the feces, the effects of enzymes and bile salts with varying pH assessed in *in vitro* experiments should be noted for more comparative and quantitative *in vivo* studies. Finally, short-term tracking (up to 48 h) following only gastrointestinal exposure was examined in this study. The *in vivo* behavior of MPs including long-term retention and effects following exposure *via* other routes (*e.g.*, inhalation, intravenous) will be of interests. Recently, oxidative stress induction

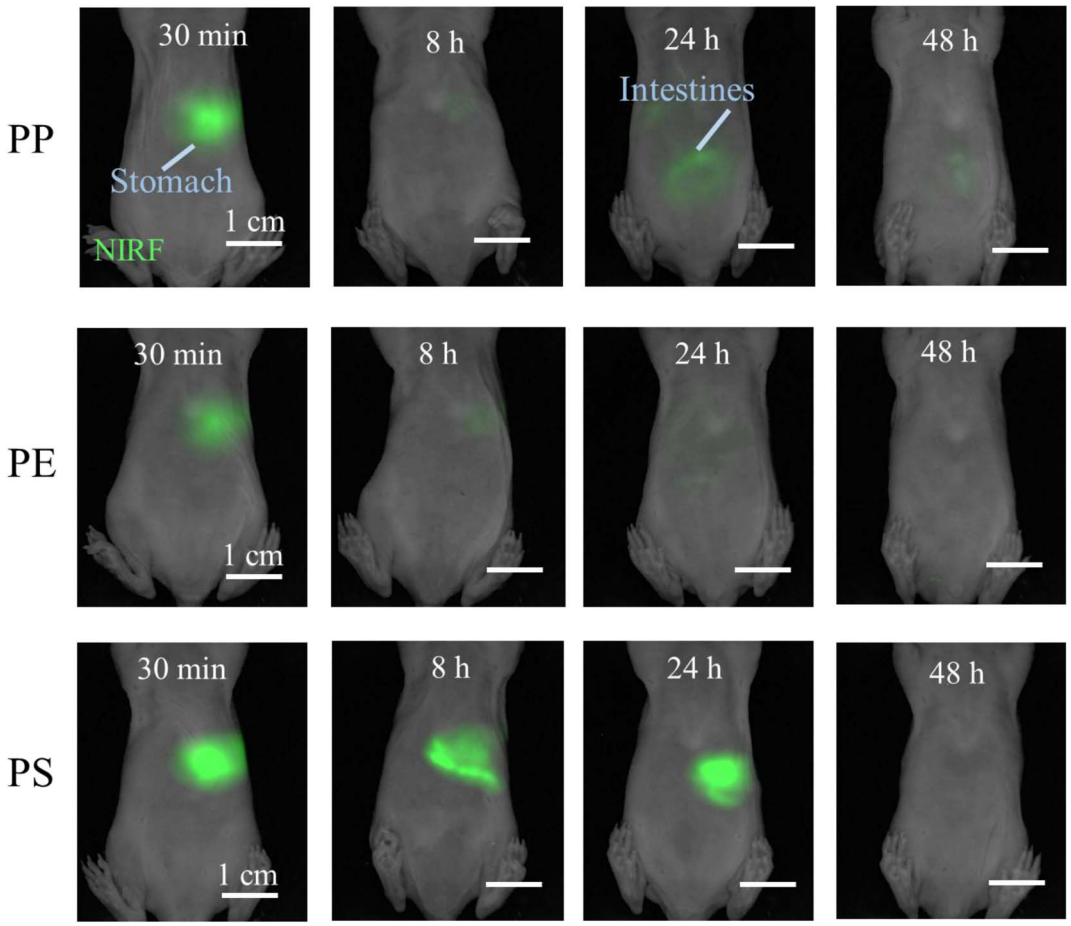

Fig. 4 *In vivo* fluorescence imaging of mice orally administered with 0.2 mL of IR-1061-loaded MPs (6 mg mL^{-1}). NIR-II fluorescence images of mice were acquired under 980 nm light irradiation (0.25 W cm^{-2}) at times ranging from 30 min to 48 h after oral administration. The peak values of size distributions for PP, PE, and PS were 57, 347, and 135 nm, respectively, as determined by DLS. Scale bar = 1 cm.

and behavioral effects of PE-MPs prepared without fluorescent labeling on *Drosophila* model was reported.[34] Future work will elucidate the differences in the potential of biological effects and toxicity by the chemical composition of MPs along with their *in vivo* distributions in other species, including mammals, to predict their risk on human health.

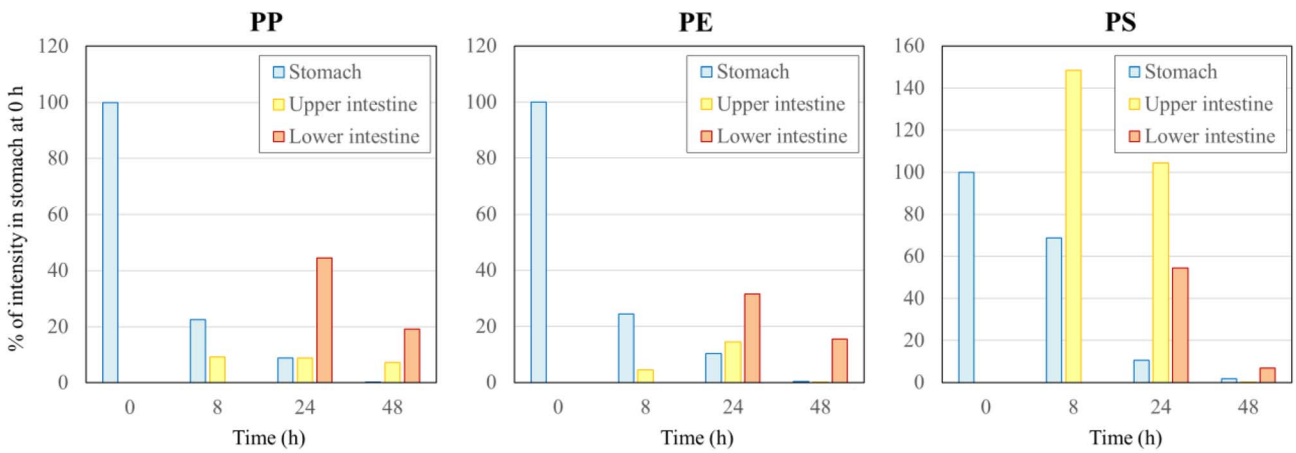

Fig. 5 Semi-quantification of time-dependent changes in the NIR-II fluorescence intensities of MPs in the gastrointestinal tract following the oral administration of the MPs. The intensities, measured for the images shown in Fig. 4, normalized by the total intensity in the stomach at 0 h (30 min post administration) are shown.

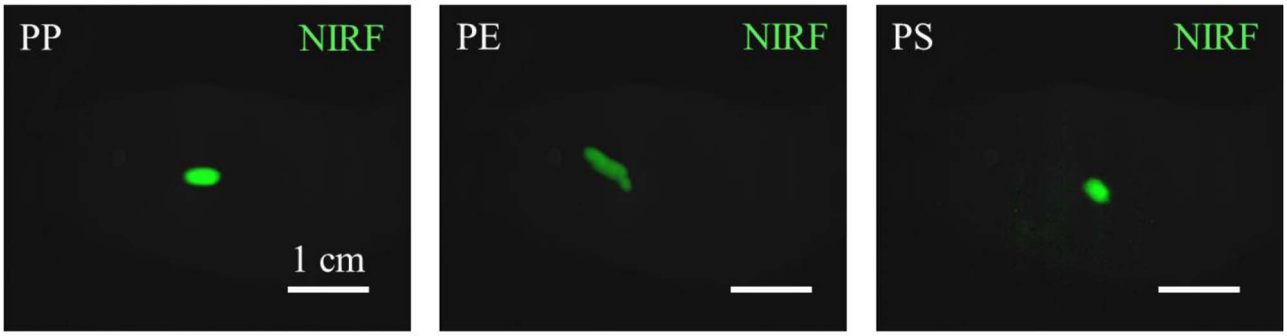

Fig. 6 Fluorescence images of feces collected 48 h after the oral administration of IR-1061-loaded MPs. NIR-II fluorescence images were acquired under 980 nm light irradiation (0.25 W cm^{-2}). Scale bar = 1 cm.

4. Conclusions

This study demonstrated a method for synthesizing IR-1061-loaded PP, PE, and PS MP models that fluoresce in the NIR-II region, enabling *in vivo* tracking of MPs. Owing to the lower polarity of PP, PE, and PS compared to PET, IR-1061 was loaded on these MPs by exploiting their thermal expansion properties; a mixture of IR-1061 in ACN and MPs was heated at 55 °C to promote the incorporation of IR-1061. The resulting IR-1061-loaded MPs facilitated real-time NIR-II fluorescence imaging, enabling the visualization of MP movement through the gastrointestinal tract and subsequent excretion in feces. Differences in intestinal retention times among MPs can be attributed to MP size rather than chemical composition. The PP particles, which were smaller in diameter (<100 nm), exhibited longer retention times in the intestine. NIR-II fluorescence imaging will contribute to elucidating the *in vivo* behavior of MPs, offering a non-invasive and highly sensitive method for assessing their biodistribution. This platform may be extended to study chronic exposure effects, different routes of entry or interactions with biological tissues. Future studies should focus on long-term tracking, toxicity assessment, and the influence of MP surface properties and morphology to better understand their environmental and health impacts.

Conflicts of interest

The authors have no conflicts of interest to declare.

Data availability

Data to reproduce the figures of this article, including the results of NIR-II fluorescence spectra and images, are available at https://tus.box.com/s/43lemcr656mg0vjlvthevuttds10v4c2.

Acknowledgements

This work is in part supported by the Japanese Society for the Promotion of Science (JSPS) KAKENHI (Grant Numbers: 22K06565, 23K24593, and 25K02871).

References

1 Y. Deng, Y. Zhang, B. Lemos and H. Ren, *Sci. Rep.*, 2017, **7**, 46687.
2 J. R. Jambeck, R. Geyer, C. Wilcox, T. R. Siegler, M. Perryman, A. Andrady, R. Narayan and K. L. Law, *Science*, 2015, **347**, 768–771.
3 X. Lim, *Nature*, 2021, **593**, 22–25.
4 A. Kukkola, A. J. Chetwynd, S. Krause and I. Lynch, *J. Hazard. Mater.*, 2024, **476**, 135053.
5 A. Nauendorf, S. Krause, N. K. Bigalke, E. V. Gorb, S. N. Gorb, M. Haeckel, M. Wahl and T. Treude, *Mar. Pollut. Bull.*, 2016, **103**, 168–178.
6 A. ter Halle, L. Ladirat, X. Gendre, D. Goudouneche, C. Pusineri, C. Routaboul, C. Tenailleau, B. Duployer and E. Perez, *Environ. Sci. Technol.*, 2016, **50**, 5668–5675.
7 J. E. Weinstein, B. K. Crocker and A. D. Gray, *Environ. Toxicol. Chem.*, 2016, **35**, 1632–1640.
8 A. H. M. E. Kabir, M. Sekine, T. Imai and K. Yamamoto, *J. Water Environ. Nanotechnol.*, 2020, **18**, 175–194.
9 A. J. Beck, M. Kaandorp, T. Hamm, B. Bogner, E. Kossel, M. Lenz, M. Haeckel and E. P. Achterberg, *Anal. Bioanal. Chem.*, 2023, **415**, 2989–2998.
10 E. S. Gruber, V. Stadlbauer, V. Pichler, K. Resch-Fauster, A. Todorovic, T. C. Meisel, S. Trawoeger, O. Hollóczki, S. D. Turner, W. Wadsak, A. D. Vethaak and L. Kenner, *Expo. Health*, 2023, **15**, 33–51.
11 K. D. Cox, G. A. Covernton, H. L. Davies, J. F. Dower, F. Juanes and S. E. Dudas, *Environ. Sci. Technol.*, 2019, **53**, 7068–7074.
12 G. O. Conti, M. Ferrante, M. Banni, C. Favara, I. Nicolosi, A. Cristaldi, M. Fiore and P. Zuccarello, *Environ. Res.*, 2020, **187**, 109677.
13 EFSA Panel on Contaminants in the Food Chain (CONTAM), *EFSA J.*, 2016, **14**, e04501.
14 S. A. Mason, V. G. Welch and J. Neratko, *Front. Chem.*, 2018, **6**, 407.
15 D. Yang, H. Shi, L. Li, J. Li, K. Jabeen and P. Kolandhasamy, *Sci. Technol.*, 2015, **49**, 13622–13627.

16 H. A. Leslie, M. J. M. van Velzen, S. H. Brandsma, A. D. Vethaak, J. Garcia-Vallejo and M. H. Lamoree, *Environ. Int.*, 2022, **163**, 107199.
17 E. L. Ng, E. H. Lwanga, S. M. Eldridge, P. Johnston, H. W. Hu, V. Geissen and D. Chen, *Sci. Total Environ.*, 2018, **627**, 1377–1388.
18 X. Yao, X. S. Luo, J. Fan, T. Zhang, H. Li and Y. Wei, *Environ. Sci.: Atmos.*, 2022, **2**, 921–942.
19 J. Wang, X. Zhao, F. Wu, L. Niu, Z. Tang, W. Liang, T. Zhao, M. Fang, H. Wang and X. Wang, *Fundam. Res.*, 2021, **1**, 317–328.
20 S. Noventa, M. S. P. Boyles, A. Seifert, S. Belluco, A. S. Jiménez, H. J. Johnston, L. Tran, T. F. Fernandes, L. Mughini-Gras, M. Orsini, F. Corami, K. Castro, F. Mutinelli, M. Boldrin, V. Puntes, M. Sotoudeh, G. Mascarello, B. Tiozzo, P. McLean, F. Ronchi, A. M. Booth, A. Koelmans and C. Losasso, *Microplast. Nanoplast.*, 2021, **1**, 9.
21 C. Fang, Y. Luo and R. Naidu, *Trends Anal. Chem.*, 2023, **166**, 117158.
22 L. Xin, M. Huang and Z. Huang, *Environ. Int.*, 2024, **187**, 108679.
23 J. Zhao, R. Lan, H. Tan, J. Wang, Y. Ma, Q. Chan, F. Jiang, Z. Wang and B. Xing, *Nat. Rev. Bioeng.*, 2025, **3**, 1019–1033.
24 A. M. Smith, M. C. Mancini and S. Nie, *Nat. Nanotechnol.*, 2009, **4**, 710–711.
25 K. Soga, M. Umezawa and K. Okubo, *Transparency in Biology*, Springer, Singapore, 2021.
26 G. Hong, S. Diao, J. Chang, A. L. Antaris, C. Chen, B. Zhang, S. Zhao, D. N. Atochin, P. L. Huang, K. I. Andreasson, C. J. Kuo and H. Dai, *Nat. Photonics*, 2014, **8**, 723–730.
27 T. Zako, M. Yoshimoto, H. Hyodo, H. Kishimoto, M. Ito, K. Kaneko, K. Soga and M. Maeda, *Biomater. Sci.*, 2015, **3**, 59.
28 L. Zhang, H. Liu, Q. Xin, L. Tang, J. Tang, Y. Liu and L. Hu, *Sci. Total Environ.*, 2023, **886**, 164033.
29 S. Inoue, T. Isobe, K. Soga and M. Umezawa, *J. Nanopart. Res.*, 2026, **28**, 5.
30 M. Umezawa, H. Kobayashi, K. Ichihashi, S. Sekiyama, K. Okubo, M. Kamimura and K. Soga, *ACS Omega*, 2022, **7**, 5817–5824.
31 M. Umezawa, Y. Ueya, K. Ichihashi, D. T. K. Dung and K. Soga, *Biomed. Mater. & Devices*, 2023, **1**, 605–617.
32 Y. Ueya, M. Umezawa, Y. Kobayashi, H. Kobayashi, K. Ichihashi, T. Matsuda, E. Takamoto, M. Kamimura and K. Soga, *ACS Nanosci. Au*, 2021, **1**, 61–68.
33 E. G. Karakolis, B. Nguyen, J. B. You, C. M. Rochman and D. Sinton, *Environ. Sci. Technol. Lett.*, 2019, **6**, 334–340.
34 S. Priscilla, R. Nagasawa, S. Senthil Kumar, S. C. Kasavaraju, C. Chandrakanth, P. Sivakumar, H. Bharat, I. Muthulingam, M. Umezawa and S. Sheik Mohideen, *Toxicology and Environmental Health Sciences*, 2025, **17**, 449–460.
35 Y. Ueya, M. Umezawa, E. Takamoto, M. Yoshida, H. Kobayashi, M. Kamimura and K. Soga, *RSC Adv.*, 2021, **11**, 18930–18937.